Exploring the potential of infrared spectroscopy in qualitative and quantitative monitoring of ovalbumin amyloid fibrillation

Jelica Milošević, Jovan Petrić, Branko Jovčić, Brankica Janković, Natalija Polović

PII: S1386-1425(19)31272-7

DOI: https://doi.org/10.1016/j.saa.2019.117882

Reference: SAA 117882

To appear in: *Spectrochimica Acta Part A: Molecular and Biomolecular Spectroscopy*

Received date: 16 July 2019

Revised date: 29 November 2019

Accepted date: 30 November 2019

Please cite this article as: J. Milošević, J. Petrić, B. Jovčić, et al., Exploring the potential of infrared spectroscopy in qualitative and quantitative monitoring of ovalbumin amyloid fibrillation, *Spectrochimica Acta Part A: Molecular and Biomolecular Spectroscopy*(2018), https://doi.org/10.1016/j.saa.2019.117882

Title: Exploring the potential of infrared spectroscopy in qualitative and quantitative monitoring of ovalbumin amyloid fibrillation

Authors: Jelica Milošević[1], Jovan Petrić[1], Branko Jovčić[2,3], Brankica Janković[1], Natalija Polović[1]*

Affiliations:

[1]University of Belgrade – Faculty of Chemistry, Department of Biochemistry, Belgrade, Republic of Serbia

[2]University of Belgrade – Faculty of Biology, Belgrade, Republic of Serbia

[3] Institute of Molecular Genetics and Genetic Engineering, University of Belgrade, Belgrade, Republic of Serbia

*__Corresponding author:__ Natalija Polovic, PhD

University of Belgrade – Faculty of Chemistry

Department of Biochemistry

Studentski trg 12 – 16

11000 Belgrade

Republic of Serbia

Phone: +381113336721

Fax: +381112184330

E-mail: polovicn@chem.bg.ac.rs

ORCID: 0000-0002-9127-2014

Abstract

Amyloid fibrils are highly ordered self-assembled (poly)peptide aggregates with cross-β structural pattern. Ovalbumin was used as a model for exploring the potential of infrared spectroscopy in detecting structural transitions and quantitative monitoring of amyloid fibrillation.

Low pH (pH 2) and high temperature (90°C) over the course of 24 hours were conditions applied for amyloid formation. Fibrillation of ovalbumin was monitored by ThT and ANS fluorescence, and SDS PAGE. A significant increase in ThT fluorescence with a plateau reached after four hours of incubation, without the lag phase, was detected. Structural transitions leading to amyloid fibrillation were analysed using all three Amide regions in ATR-FTIR spectra. Significant changes were detected in Amide I and Amide III region (decrease of α-helix and increase of β-sheet peaks). To establish a fast, precise and simple method for quantitative monitoring of amyloid fibrillation, the Amide I/Amide II ratios of aggregation specific β-sheets (1625 and 1695 cm^{-1}, respectively) with 1540 cm^{-1} as internal standard were used, resulting in good correlation (R^2 = 0.93 and 0.95) with the data observed by monitoring ThT fluorescence. On the other hand, assessing aggregation specific β-sheet contents by self-deconvolution showed lower correlation with ThT fluorescence (R^2 = 0.75 and 0.64).

Here we examined structural transitions during ovalbumin fibrillation in a qualitative and quantitative manner by exploiting the full potential of Amide regions simultaneously. Secondary structure distribution was monitored using second derivative spectra in Amide I region. A novel, simple mathematical calculation for quantitative monitoring of fibrils formation was presented employing that the increase in low and high frequency aggregation specific β-sheet in Amide I region compared to the internal standard in Amide II region is suitable for fibril formation monitoring.

Keywords: ovalbumin, amyloid fibrils, ATR-FTIR, secondary structures, Amide I/Amide II ratio

1. Introduction

Amyloid fibrils are highly ordered self-assembled aggregates which represent the most stable structural state for proteins and polypeptides. When found *in vivo*, amyloid fibrils are often associated with pathological conditions such as Alzheimer's or prion disease, but the ability to form amyloid fibrils appears to be an intrinsic property of all proteins and protein fragments *in vitro* [1]. Fibrils are usually composed of at least two protofilaments that twist around one another to form a cross-β-sheet structure [2]. Since amyloids display exceptional chemical and mechanical stability, resistance to proteolytic degradation, detergents and high temperatures, they represent interesting substitute to synthetic materials used in biotechnology [3].

In vitro conditions for fibril formation show a high degree of diversity. Varying parameters include protein concentration, pH, ionic strength, temperature, and incubation time. There is not a single path leading to amyloid formation as it is considered as a global minimum of protein folding funnel [2, 4, 5]. Destabilization of protein monomers leads to the formation of nuclei for fibrillation. These nuclei appear to resemble monomeric proteins in the molten globule state [6] with much experimental evidence on diverse model systems supporting this thesis [7-9]. Metastable oligomers form rod or worm-like protofibrils which assemble to protofilaments - single-stranded fibrils which twist helically to form mature fibrils of varying sizes Dobson 2017 [4]. While shorter forms can have lengths less than 100 nm, longer forms exceed 1μm [10]. Common characteristics that classify these structures as amyloid fibrils include the diameter of about 10 nm, high level of the β-sheet structure, cross-β diffraction pattern, and hydrogen exchange resistant core [10].

Ovalbumin is a structural protein from serpin superfamily which represents more than 50% of egg-white proteins. It is an acidic protein with an isoelectric point of 4.6 and 45 kDa molecular weight. The native state of ovalbumin is characterized as a combination of α-helix and β-sheet secondary structures [11]. Being abundant, stabile and accessible, ovalbumin is used in both, science and technology as an emulsifier, gelling agent as well as a matrix for *in ovo* experiments which *in vitro* simulate high-protein concentration conditions. Molten globule as a stable intermediate in

ovalbumin folding/unfolding is formed at low pH conditions [12-14]. Even though all proteins described in the amyloid state can reach it in different conditions, in the case of ovalbumin, a low pH of about 2 and high temperature in a prolonged period are almost universal conditions applied for its fibrillation [15-18].

A few experimental techniques are set as standards for amyloid fibril analysis. These include: binding specific fluorescent dyes - Thioflavin T (ThT) and Congo red and shifting their fluorescent spectra; secondary-structure dependent spectroscopy techniques such as circular dichroism (CD) and infrared spectroscopy (IR), and Raman spectroscopy [19]; electron and atomic-force microscopy techniques [20]; X-ray scattering techniques [21-23]. Even though ThT binding is taken as the most specific evidence for amyloid forms, ThT does not only bind to amyloid fibrils. ThT supposedly recognizes the groove on a fibrillar structure, so it can also bind DNA, cyclodextrins, SDS. These interfering substances can make false results, especially in biological samples. Interaction is also pH, ionic strength and viscosity dependent. [10].

In the past few years, IR techniques are revised as a promising tool for monitoring of amyloid fibril formation [24, 25]. Determination of secondary structure content based on peak distribution in the Amide I region has a long tradition in protein secondary structure analysis [26-28]. Besides the ability to handle insoluble protein samples, IR has an important additional advantage over CD spectroscopy as it can discriminate between native-like and aggregation specific β-sheet [20]. By now, other spectroscopy techniques (except Raman spectroscopy) have not shown this ability and IR analyses are the fastest, cheapest and easiest way to analyse the samples and to quantitatively monitor the change in secondary structure distribution during the fibrillation process.

The aim of this manuscript was to exploit the potential of ATR-FTIR in detecting structural transitions that lead to ovalbumin amyloid formation. The second goal was to establish a facile and precise procedure for the quantitative monitoring of the amyloid fibrillation process.

2. Materials and methods

2.1 Materials

Thioflavin T, 8-Anilinonaphthalene-1-sulfonic acid (ANS), Bovine serum albumin (BSA) were purchased from Sigma–Aldrich (Steinheim, Germany). Coomassie brilliant blue R-250 (CBB R-250) was purchased from Serva (Heidelberg, Germany). Unstained protein molecular weight markers were purchased from Thermo Scientific (Rockford, IL, USA). The rest of the chemicals were analytical grade commercial products used without further purification.

2.2 Protein purification

Ovalbumin was isolated in two steps from the hen egg white. First, globulins were precipitated at 50% saturation of ammonium sulphate. The precipitate was removed after a 30-minute centrifugation step at 3000 x g. Ovalbumin was precipitated from the supernatant by adjusting the pH to its isoelectric point – 4.6 with 2 M acetic acid. The precipitate was separated by centrifugation (30 minutes at 3000 x g) and resuspended in 50 mM Tris buffer pH 7 in which the protein was stored at -20°C. Protein concentration was determined by the Bradford method with bovine serum albumin (BSA) as a standard [29]. The purity of ovalbumin preparation was analysed by reverse-phase high-performance liquid chromatography (RP-HPLC) performed on an Äkta Purifier 10 system (GE Healthcare, Uppsala, Sweden) with a Discovery BIO Wide Pore C5 column (10 cm by 4.6 mm; particle size, 5m; Supelco, Bellefonte, PA, USA). Acetonitrile gradient was used for elution (0 to 90% of acetonitrile with 0.1% trifluoroacetic acid in 10 column volumes). Absorbance at 215 nm was monitored.

2.3 Destabilization and fibrils preparation

A buffer system of ovalbumin solution was exchanged on a Sephadex G-25 column. Instead of 50 mM Tris buffer pH 7, pH 2 Mili-Q water (pH adjusted with 2 M HCl) was used in order to destabilize the protein and favour the molten globule state [12, 16]. Protein samples of 6 mg/mL

[30] were incubated for 24 h at 90°C in dry heating block BioSan CH-100. Fibrillation was monitored by measuring ThT and ANS fluorescence of aliquots taken at different time points (0.5, 1, 2, 4, 8, 12, 16, 20 and 24 hours).

2.4 SDS-PAGE

SDS PAGE was used for the analysis of protein purity as well as for the comparison of ovalbumin samples during the fibrillation process. The amounts of 1 μg of proteins were analysed by sodium dodecyl sulphate-polyacrylamide gel electrophoresis (SDS PAGE) under reducing conditions according to Laemmli (1970) using Hoefer Dual Gel Mighty Small SE 245 vertical electrophoresis system (Hoefer, Holliston, MA, USA) [31]. Electrophoretic gels were stained with Coomassie Brilliant Blue R-250 (Serva, Heidelberg, Germany).

2.5 ThT and ANS fluorescence measurements

Fluorescent dyes were dissolved in concentrations 0.1 mM (ThT) and 8 mM (ANS) in 100 mM Tris-HCl buffer pH 8.5. ThT fluorescence reaction mixtures contained 20 μL of protein samples in 0.06 mg/mL concentration, 180 μL of 100 mM Tris-HCl buffer pH 8.5 and 20 μL of ThT solution. The excitation wavelength was 440 nm, and the emission wavelength was 480 nm. ANS fluorescence reaction mixture contained 10 μL of protein samples (0.06 mg/mL), 190 μL of 100 mM Tris-HCl buffer pH 8.5 and 20 μL of ANS solution. Excitation and emission wavelengths were set to 390 and 480 nm, respectively. Tecan Infinite m200 PRO was used for fluorescence measurements in 96-well plates.

2.6 Fourier transform infrared spectroscopy (FTIR)

Infrared spectra were collected using Fourier transform infrared spectroscopy (FTIR) with an attenuated total reflectance (ATR) at 1 cm^{-1} resolution (Nicolet 6700 FTIR placed in instrument chamber, software OMNIC, Version 7.0, Thermo Scientific, USA) using DTGS KBr detector with

thermoelectric (TE) cooling. Liquid samples (1.5 μL) were intensively vortexed and applied on a diamond crystal (Smart Orbit, Thermo Scientific, USA) and evaporated to thin ATR films using the stream of argon. Spectra of starting ovalbumin sample and samples heated for 0.5, 1, 2, 4, 8, 12, 16, 20 and 24 hours were collected in 64 scans. OMNIC software was used for automatic ATR correction, automatic baseline correction, and automatic smooth, according to manufacturer's instructions. Background spectra were collected before and after each sample spectrum.

Amide I, Amide II and Amide III regions of all samples were analysed. Specific peaks were identified based on the second-derivative spectra and assigned to particular secondary structures.

2.7 Calculations

Spectral signals (absorbance) in recorded spectra were used for calculation of Amide I / Amide II ratios.

Fourier self-deconvolution and second derivative spectra were used to resolve the spectra to its Savitzky-Golay constituents by automatic peak resolve function in OMNIC software. Total area under peak curves attributed to certain secondary structure within Amide I region was calculated by summation of individual peak areas. Contents of aggregation specific secondary structures were calculated as a percentage of total Amide I area.

Plots presented in the manuscript are made using Origin software.

Secondary structure content of ovalbumin determined by X-ray diffraction [32] was calculated from UniProt entry [https://www.uniprot.org/uniprot/P01012] from the chain without signal peptide.

2.8 Atomic Force Microscopy (AFM)

Aliquotes of 24 hours-incubated ovalbumin samples were scanned using AFM in tapping-mode (BioScope Resolve, Bruker, Germany). Solutions were diluted to 1 mg/mL and incubated for 2 minutes on Mica discs (model SD-101, Bruker, Germany), rinsed with Mili-Q water, and dried with

the stream of nitrogen. Nanoscope 8.10 software was used for the analysis of images, including fibril length measurements.

3 Results and discussion

3.1 Purification of ovalbumin from egg white

In order to obtain a low cost - high yield ovalbumin preparation, crude ovalbumin was purified from egg white using salt precipitation of globulins and consequent precipitation of ovalbumin by pH change. Purification was monitored by SDS-PAGE (Figure 1a) and RP-HPLC (Figure 1b). Purity was calculated from reverse-phase chromatogram by comparing ovalbumin peak area and peak areas of impurities using Unicorn software and it was found to be around 80%.

3.2 Amyloid fibrils preparation and characterization

Amyloid fibrils were prepared by a combination of acidic pH and thermal destabilization [15, 16] over the course of 24 hours. Fibrillation process was monitored by ThT fluorescence measurement (results shown in Figure 2a). Surface hydrophobicity during the incubation period was examined by ANS fluorescence measurement (Figure 2b). Our results show a significant increase in both, ThT and ANS fluorescence during the first hour of incubation. ThT fluorescence reached a plateau after four hours of incubation without the detectable lag phase which is not a single case reported [30]. The increase in ThT fluorescence, which is the most commonly used indicator of amyloid fibrils formation, was in agreement with previously reported data [2, 16, 30]. As ThT does not bind equally to all forms of fibril intermediates, the increase in ThT fluorescence to end-point level was taken as the sufficient evidence of mature fibrils formation. It was already reported that ovalbumin fibrillation upon heating is initially accompanied by negative hydration which increases surface hydrophobicity and consequentially ANS fluorescence [2], which is in concordance with data presented in Figure 2b (first 4 hours). However, mature ovalbumin fibrils showed ANS fluorescence decrease [33-35] as detected in the time range 16-24 hours. AFM microscopy of the sample

incubated 24 hours at 90°C was employed to confirm fibrillation and it showed short mature fibrils with diameters of about 10 nm and the length range 50-200 nm (Figure 2c).

Fibrils are shown to be stabile upon sample preparation for SDS-PAGE (Figure 3a). The starting sample has a dominant band at about 45 kDa corresponding to the ovalbumin monomer. After 2 hours of incubation at 90°C, the monomer ovalbumin band is still present which indicates the existence of an equilibrium between fibril forms and soluble protein monomers [36]. The indiscrete electrophoretic pattern with smear in the low-molecular-weight region is likely to be the result of ovalbumin fragmentation at low-pH, high-temperature conditions, as suggested by Lara et al [16]. After 24 hours of incubation, a dominant band is present at the midpoint of stacking and running gels which is an additional indicator of high molecular weight fibrillar forms resistant to denaturing conditions in the presence of SDS and β-mercaptoethanol at increased temperature [37-39]. Densitometric analysis of the monomer ovalbumin band (Figure 3b) showed an inverse trend to the ThT fluorescence curve (Figures 2a).

3.3 Qualitative ATR-FTIR analyses of treated ovalbumin samples

After confirming that the applied procedure yielded the mature fibrils of ovalbumin, our next goal was to further characterize the ovalbumin fibril formation process at pH 2 and 90°C in a more detailed, structural sense.

3.3.1 Amide I region

Amide I region which spreads in 1600-1700 cm^{-1} range is the most sensitive region of the IR spectrum for protein secondary structure analysis. It arises from C=O stretching vibrations of peptide bonds with less significant contribution of the out-of-phase CN stretching vibration, the CCN deformation and the NH in-plane bend [28]. Predominant structural features that characterize amyloids are β-sheets; more precisely aggregation specific intermolecular β-sheet usually predominates.

A simple comparison of the Amide I spectra of ovalbumin samples incubated for different time intervals suggests large structural rearrangements especially pronounced in the region around 1653 and 1625 cm^{-1} (Figure 4) indicating the decrease in α-helix content and increase in aggregation specific β-sheet content.

Even a qualitative examination of spectra shows significant blue-shift during thermal treatment. Peaks attributed to native-like structures (α-helix, random coil, and native-like β-sheet) began to disappear in favour of aggregation specific β-sheet bands, especially low-frequency band (1625 cm^{-1}). Aggregation specific β-sheet rises shortly after ovalbumin exposure to high temperature while a significant drop in secondary structures happens after 24-hour incubation. A similar phenomenon - β-shift was observed in the studies focused on ovalbumin fibrillation induced by high temperature, but after prolonged time period [16, 40] and in ovalbumin fibrillation induced by acetonitrile and trifluoroacetic acid [34, 41].

In order to clarify the presence and change in otherwise overlapped secondary structure bands, second derivative spectra in Amide I region were used (Figure 5).

The most prominent minima of unheated ovalbumin sample second derivative spectrum were attributed to the most abundant native-like secondary structures according to previously published data: native-like β-sheet (1636 cm^{-1}) [33, 42], random coil (1646 cm^{-1}) [42], α-helix (1653 cm^{-1}) [42], unordered structures (1662-1675 cm^{-1}) [43], β-turn (1683 cm^{-1}) [44]. Additional bands, barely visible in starting ovalbumin sample were identified as side chain peak (1611 cm^{-1}) and low-frequency and high frequency aggregation specific β-sheets (1625 and 1695 cm^{-1}, respectively) [16, 17, 20, 28]. Second derivatives of spectra in Amide I region presented in Figure 5 show differences in bands attributed to the main ordered secondary structures of ovalbumin.

Second derivative spectra of the starting, unheated ovalbumin sample shows prominent local minima corresponding to native-like secondary structures, such as α-helix detected at 1653 cm^{-1}. During first 4 hours of incubation at 90°C, this band's intensity is decreasing, partly on the count of

transition unordered structures which appear with lower intensities on higher and lower wavenumbers (at around 1662 and 1646 cm^{-1}), and partly on the count of two increasing aggregation specific minima at 1625 and 1695 cm^{-1}. These minima correspond to the low-frequency and high frequency aggregation specific β-sheets, characteristic in spectra of amyloid forms. They first appear in the second derivative of the spectrum acquired after only 0.5 hours of high-temperature incubation and become more prominent during incubation time.

In the period 8-24 hours of incubation, the same trend is observed. Local minima of native-like secondary structures are further decreasing, and become barely visible in the derivative spectra of 20 and 24 hours heated ovalbumin. This results in the derivative spectra in which the only prominent bands are those attributed to low- and high-frequency aggregation specific β-sheets (Figure 5). Thus second derivative spectra provide even more straight-forward qualitative evidence for amyloid formation, and additionally, precise guidelines for the position of the bands that can be attributed to aggregation specific secondary structures that are under transition in the fibrillation process.

3.3.2 Amide II region

Changes in the Amide II region are less pronounced. The maximum at 1535-1540 cm^{-1} was detected in all samples (Figure 6). Major contributors to Amide II region are NH in-plane bend and CN stretching vibrations which are less conformation dependant [25, 28, 45], which explains almost overlapping spectra of samples with significant secondary structure changes indicated in Amide I region. The sensitivity of Amide II region is generally regarded as lower and it is commonly used as the internal standard for comparison of relative Amide I/Amide II intensities when analysing secondary structure content in differently treated samples [45, 46]. After revealing that the Amide II region cannot provide significant information about the secondary structure changes, it has been used as an internal standard in this study (see below).

3.3.3 Amide III region

Recent FTIR studies have suggested the potential of rarely used Amide III region for protein structure analysis. Even though the Amide III region (1200-1350 cm^{-1}) has been usually considered as the least convenient for polypeptide conformation analysis because of its low absorption compared to the other two Amide regions, its advantages predominate when applied to high protein concentrations. The main advantage over the most frequently used Amide I region is the resolution of secondary structure absorption bands which clearly speaks for the huge potential of this spectral region. Amide III region arises as a combination of the NH bending and the CN stretches vibrations. There is a small contribution of the CO in-plane bending and the CC stretching vibration [24, 28]. Using Amide III region for amyloid fibrils formation monitoring has fewer drawbacks as the samples are highly concentrated, and on the other hand, secondary structure changes are prominent so sensitivity is not an issue. The position of α-helix in Amide III region is assigned to 1320 cm^{-1}, while a turn is recognized at about 1270-1285 cm^{-1} (between 1260-1280 cm^{-1} in literature [24]). β-sheet structures are positioned at about 1235 cm^{-1} in the starting samples, while blue shift towards 1230 cm^{-1} can be detected during fibrillation. The intensity of a band at 1,220-1,240 cm^{-1} was already assigned to β-sheet [25]. Changes in Amide III region shown in Figure 7 are consistent to those observed within Amide I region and appear to be even more prominent when analysed vaguely by qualitative comparison. Still, Amide III region is restricted to qualitative analysis while Amide I region can provide the information about the relative contribution of different secondary structures, with the additional advantage of discriminating between intra- and intermolecular β-sheets.

3.4 Quantitative analysis of secondary structure transitions by ATR-FTIR

3.4.1 Deconvolution of Amide I region

For quantitative analysis of structural transitions which lead to amyloid formation, spectra of all samples in Amide I region were deconvoluted and their aggregation specific secondary structure

content was determined. We already used it to describe secondary structure changes during cold denaturation of papain and trypsin [26, 47]. Despite complexity in mathematical operations used during deconvolution of Amide I region, it has been used by many authors to describe structural transitions following amyloid fibrillation [25, 48-50]. Recently, Ruggeri and co-workers applied Amide I region deconvolution to estimate the secondary structure content of Josephin domain of ataxin-3 which served to prove the native state of non-treated sample and to distinguish it from thermally treated sample proved to occupy amyloid state by multiple techniques [19].

Secondary structure content of ovalbumin sample in neutral conditions (pH7) was comparable to secondary structure content calculated from its crystal structure [32] (shown in brackets) and is found to be: β-sheets in total 36% (37.9); α-helix 26% (26.3); β-turn 7% (7.7), and all unordered structures 31% (28.1) proving that deconvolution procedure produces native-like secondary structure content of native ovalbumin sample. Deconvoluted spectrum of ovalbumin at pH 7 is shown in Supplementary figure S1. Initial change of pH of ovalbumin solution from 7 to 2 results in some secondary structures perturbations regarding slight blue shift of the entire spectrum (Supplementary figure S2).

Automatic self-deconvolution was then used for the comparative aggregation specific β-sheet content analysis between treated samples (Supplementary Files 3-12). Since second derivative spectra suggested that majority of native-like secondary structures disappear and shift after only 0.5 hours of incubation, transient secondary structures detected between 1625 and 1695 cm^{-1} were not quantitatively analysed, respectively. Figure 8 shows that around 33% of detected structures in the 24h sample are in amyloid-like secondary structures, while the rest (67%) assume transient conformations. It has been already shown in the case of lysozyme amyloid fibrils that parts of the primary structure that does not form fibrils under investigated fibrillation conditions are prone to hydrolyse from the fibril [49] which could explain fragmentation observed both in Figure 3 and by Lara et al [16].

The curves showing the increase in aggregation specific β-sheet content during incubation time (Figure 8a and b) have the same shape as ThT fluorescence curve, supporting the stand that IR is a suitable method for amyloid formation monitoring. However, the correlation of these trends was not very pronounced (Figure 8c and d), which prompted us to take a different approach in quantitative analysis of IR data.

3.4.2 Amide I/Amide II ratio

As it was already mentioned, the position of maximum in the Amide II region (the absorption band at 1540 cm^{-1}) does not change upon denaturation and fibrillation, both in this work and as reported by Bothelo et al [22], it was chosen as an internal standard for normalization the intensities of aggregation specific β-sheet bands in order to quantitatively compare different samples in Amide I region of IR spectra. To establish a fast and simple method for estimation of intensities of aggregation specific β-sheet during the incubation period, we plotted the Amide I/Amide II ratios of both, low and high frequency aggregation β-sheets with 1540 cm^{-1} (as internal standard), for samples with different incubation interval and obtained the curves presented in Figure 9a and 9b. These curves also suggest that the critical step in amyloid formation takes place in the first four incubation hours and by 24 hours at 90°C, a plateau is reached. The same trend is proved by ThT fluorescence (Figure 2), implying that Amide I/Amide II ratio can be used for quantitative monitoring of amyloid fibrillation. Furthermore, ThT fluorescence and both low- and high-frequency aggregation specific bands intensities normalized using Amide II maxima showed high correlation (R^2 0.934 and 0.955, respectively), Figure 9c and 9d.

4 Conclusions

ATR FTIR technique is particularly useful for the analysis of insoluble protein samples e.g. membrane proteins and amyloid fibrils, which are not compatible with other spectroscopy techniques. Here we used ovalbumin amyloid fibrils as a model for exploring the full potential of

simultaneous analysis of Amide regions. Ovalbumin amyloid formation at low-pH, high temperature conditions has been extensively investigated in structural sense.

Firstly, using conventional techniques (ThT fluorescence and AFM) we confirmed that our procedure for fibril formation has yielded mature fibrils.

By the extensive analysis of all three Amide regions, it is possible to obtain the data about global secondary structure transitions which are in a good agreement from both, Amide I and Amide III regions. Amide II region can be employed as an internal reference for normalizing band intensities within Amide I region.

We showed that comparison of Amide I/Amide II ratio of aggregation specific bands is in correlation with the trend obtained by conventional ThT fluorescence monitoring, thus proving its potential in fast screening of amyloid presence with potential use in biological samples analysis.

Acknowledgements

This work was financially supported by the Ministry of Education, Science and Technological Development, Republic of Serbia, Grant no. 172049.

References

[1] C.M. Dobson, Protein folding and misfolding, Nature, 426 (2003) 884-890.

[2] F. Chiti, C.M. Dobson, Protein Misfolding, Amyloid Formation, and Human Disease: A Summary of Progress Over the Last Decade, Annu Rev Biochem, 86 (2017) 27-68.

[3] I. Cherny, E. Gazit, Amyloids: not only pathological agents but also ordered nanomaterials, Angew Chem, 47 (2008) 4062-4069.

[4] A.K. Buell, C.M. Dobson, T.P. Knowles, The physical chemistry of the amyloid phenomenon: thermodynamics and kinetics of filamentous protein aggregation, Essays Biochem, 56 (2014) 11-39.

[5] Y. Cordeiro, B. Macedo, J.L. Silva, M.P.B. Gomes, Pathological implications of nucleic acid interactions with proteins associated with neurodegenerative diseases, Biophys Rev, 6 (2014) 97-110.

[6] M. Stefani, C.M. Dobson, Protein aggregation and aggregate toxicity: new insights into protein folding, misfolding diseases and biological evolution, J Mol Med-Jmm, 81 (2003) 678-699.

[7] G. Agocs, B.T. Szabo, G. Kohler, S. Osvath, Comparing the folding and misfolding energy landscapes of phosphoglycerate kinase, Biophys J, 102 (2012) 2828-2834.

[8] L. Skora, S. Becker, M. Zweckstetter, Molten globule precursor states are conformationally correlated to amyloid fibrils of human beta-2-microglobulin, J Am Chem Soc, 132 (2010) 9223-9225.

[9] M.M. Pedrote, G.A.P. de Oliveira, A.L. Felix, M.F. Mota, M.A. Marques, I.N. Soares, A. Iqbal, D.R. Norberto, A.M.O. Gomes, E. Gratton, E.A. Cino, J.L. Silva, Aggregation-primed molten globule conformers of the p53 core domain provide potential tools for studying p53C aggregation in cancer, J Biol Chem, 293 (2018) 11374-11387.

[10] K. Gade Malmos, L.M. Blancas-Mejia, B. Weber, J. Buchner, M. Ramirez-Alvarado, H. Naiki, D. Otzen, ThT 101: a primer on the use of thioflavin T to investigate amyloid formation, Amyloid, 24 (2017) 1-16.

[11] H.Y. Hu, H.N. Du, alpha-to-beta structural transformation of ovalbumin: Heat and pH effects, J Protein Chem, 19 (2000) 177-183.

[12] E. Tatsumi, M. Hirose, Highly ordered molten globule-like state of ovalbumin at acidic pH: Native-like fragmentation by protease and selective modification of Cys367 with dithiodipyridine, J Biochem, 122 (1997) 300-308.

[13] M. Sogami, S. Era, T. Koseki, N. Nagai, Structural characterization of the molten globule and native states of ovalbumin: A H-1 NMR study, J Pept Res, 50 (1997) 465-474.

[14] M. Bhattacharya, S. Mukhopadhyay, Structural and dynamical insights into the molten-globule form of ovalbumin, J Phys Chem B, 116 (2012) 520-531.

[15] L.M.C. Sagis, C. Veerman, E. van der Linden, Mesoscopic properties of semiflexible amyloid fibrils, Langmuir, 20 (2004) 924-927.

[16] C. Lara, S. Gourdin-Bertin, J. Adamcik, S. Bolisetty, R. Mezzenga, Self-assembly of ovalbumin into amyloid and non-amyloid fibrils, Biomacromolecules, 13 (2012) 4213-4221.

[17] M. Bhattacharya, N. Jain, P. Dogra, S. Samai, S. Mukhopadhyay, Nanoscopic Amyloid Pores Formed via Stepwise Protein Assembly, J Phys Chem Lett, 4 (2013) 480-485.

[18] Y. Sugimoto, Y. Kamada, Y. Tokunaga, H. Shinohara, M. Matsumoto, T. Kusakabe, T. Ohkuri, T. Ueda, Aggregates with lysozyme and ovalbumin show features of amyloid-like fibrils, Biochem Cell Biol, 89 (2011) 533-544.

[19] D. Kurouski, R.P. Van Duyne, I.K. Lednev, Exploring the structure and formation mechanism of amyloid fibrils by Raman spectroscopy: a review, Analyst, 140 (2015) 4967-4980.

[20] J.S. Cristovao, B.J. Henriques, C.M. Gomes, Biophysical and Spectroscopic Methods for Monitoring Protein Misfolding and Amyloid Aggregation, Methods Mol Biol, 1873 (2019) 3-18.

[21] D.S. Eisenberg, M.R. Sawaya, Structural Studies of Amyloid Proteins at the Molecular Level, Annu Rev Biochem, 86 (2017) 69-95.

[22] K.L. Morris, L.C. Serpell, X-ray fibre diffraction studies of amyloid fibrils, Methods Mol Biol, 849 (2012) 121-135.

[23] C.M. Dobson, Biophysical Techniques in Structural Biology, Annu Rev Biochem, Vol 88, 88 (2019) 25-33.

[24] K. Cai, X. Zheng, J. Liu, F. Du, G. Yan, D. Zhuang, S. Yan, Mapping the amide-I vibrations of model dipeptides with secondary structure sensitivity and amino acid residue specificity, and its application to amyloid beta-peptide in aqueous solution, Spectrochim Acta A, 219 (2019) 391-400.

[25] J. Seo, W. Hoffmann, S. Warnke, X. Huang, S. Gewinner, W. Schollkopf, M.T. Bowers, G. von Helden, K. Pagel, An infrared spectroscopy approach to follow beta-sheet formation in peptide amyloid assemblies, Nat Chem, 9 (2017) 39-44.

[26] B. Raskovic, M. Popovic, S. Ostojic, B. Andelkovic, V. Tesevic, N. Polovic, Fourier transform infrared spectroscopy provides an evidence of papain denaturation and aggregation during cold storage, Spectrochim Acta A, 150 (2015) 238-246.

[27] W. Mantele, The analysis of protein conformation by infrared spectroscopy: an introduction of the editor to a scientific dispute, Spectrochim Acta A, 138 (2015) 964-966.

[28] A. Barth, Infrared spectroscopy of proteins, Biochim Biophys Acta, 1767 (2007) 1073-1101.

[29] M.M. Bradford, A rapid and sensitive method for the quantitation of microgram quantities of protein utilizing the principle of protein-dye binding, Anal Biochem, 72 (1976) 248-254.

[30] J.M. Kalapothakis, R.J. Morris, J. Szavits-Nossan, K. Eden, S. Covill, S. Tabor, J. Gillam, P.E. Barran, R.J. Allen, C.E. MacPhee, A kinetic study of ovalbumin fibril formation: the importance of fragmentation and end-joining, Biophys J, 108 (2015) 2300-2311.

[31] U.K. Laemmli, Cleavage of structural proteins during the assembly of the head of bacteriophage T4, Nature, 227 (1970) 680-685.

[32] M. Yamasaki, N. Takahashi, M. Hirose, Crystal structure of S-ovalbumin as a non-loop-inserted thermostabilized serpin form, J Biol Chem, 278 (2003) 35524-35530.

[33] A. Iram, A. Naeem, Existence of Different Structural Intermediates and Aggregates on the Folding Pathway of Ovalbumin, J Fluoresc, 22 (2012) 47-57.

[34] A. Naeem, S. Amani, Deciphering Structural Intermediates and Genotoxic Fibrillar Aggregates of Albumins: A Molecular Mechanism Underlying for Degenerative Diseases, PloS one, 8 (2013).

[35] A. Iram, A. Naeem, Conformational Transitions Provoked by Organic Solvents in Chicken Egg Ovalbumin: Mimicking the Local Environment, Protein J, 32 (2013) 7-14.

[36] T. Urbic, S. Najem, C.L. Dias, Thermodynamic properties of amyloid fibrils in equilibrium, Biophys Chem, 231 (2017) 155-160.

[37] R. Sarroukh, E. Cerf, S. Derclaye, Y.F. Dufrene, E. Goormaghtigh, J.M. Ruysschaert, V. Raussens, Transformation of amyloid beta(1-40) oligomers into fibrils is characterized by a major change in secondary structure, Cell Mol Life Sci, 68 (2011) 1429-1438.

[38] E. Cerf, R. Sarroukh, S. Tamamizu-Kato, L. Breydo, S. Derclaye, Y.F. Dufrene, V. Narayanaswami, E. Goormaghtigh, J.M. Ruysschaert, V. Raussens, Antiparallel beta-sheet: a signature structure of the oligomeric amyloid beta-peptide, Biochem J, 421 (2009) 415-423.

[39] A. Itkin, V. Dupres, Y.F. Dufrene, B. Bechinger, J.M. Ruysschaert, V. Raussens, Calcium ions promote formation of amyloid beta-peptide (1-40) oligomers causally implicated in neuronal toxicity of Alzheimer's disease, PloS one, 6 (2011) e18250.

[40] N. Tanaka, Y. Morimoto, Y. Noguchi, T. Tada, T. Waku, S. Kunugi, T. Morii, Y.F. Lee, T. Konno, N. Takahashi, The mechanism of fibril formation of a non-inhibitory serpin ovalbumin revealed by the identification of amyloidogenic core regions, J Biol Chem, 286 (2011) 5884-5894.

[41] A. Naeem, T.A. Khan, M. Muzaffar, S. Ahmad, M. Saleemuddin, A partially folded state of ovalbumin at low pH tends to aggregate, Cell Biochem Biophys, 59 (2011) 29-38.

[42] A.C. Dong, J.D. Meyer, J.L. Brown, M.C. Manning, J.F. Carpenter, Comparative Fourier transform infrared and circular dichroism spectroscopic analysis of alpha(1)-proteinase inhibitor and ovalbumin in aqueous solution, Arch Biochem Biophys, 383 (2000) 148-155.

[43] G. Vedantham, H.G. Sparks, S.U. Sane, S. Tzannis, T.M. Przybycien, A holistic approach for protein secondary structure estimation from infrared spectra in H2O solutions, Anal Biochem, 285 (2000) 33-49.

[44] D. Smith, V.B. Galazka, N. Wellner, I.G. Sumner, High pressure unfolding of ovalbumin, Int J Food Sci Tech, 35 (2000) 361-370.

[45] J. Buijs, W. Norde, J.W.T. Lichtenbelt, Changes in the Secondary Structure of Adsorbed IgG and F(ab‘)2Studied by FTIR Spectroscopy, Langmuir, 12 (1996) 1605-1613.

[46] T.-H. Lee, S.-Y. Lin, Additives affecting thermal stability of salmon calcitonin in aqueous solution and structural similarity in lyophilized solid form, Process Biochem, 46 (2011) 2163-2169.

[47] B. Rašković, S. Vatić, B. Anđelković, V. Blagojević, N. Polović, Optimizing storage conditions to prevent cold denaturation of trypsin for sequencing and to prolong its shelf life, Biochem Eng J, 105 (2016) 168-176.

[48] M.F. Mossuto, A. Dhulesia, G. Devlin, E. Frare, J.R. Kumita, P.P. de Laureto, M. Dumoulin, A. Fontana, C.M. Dobson, X. Salvatella, The Non-Core Regions of Human Lysozyme Amyloid Fibrils Influence Cytotoxicity, J Mol Biol, 402 (2010) 783-796.

[49] E. Frare, M.F. Mossuto, P.P. de Laureto, S. Tolin, L. Menzer, M. Dumoulin, C.M. Dobson, A. Fontana, Characterization of Oligomeric Species on the Aggregation Pathway of Human Lysozyme, J Mol Biol, 387 (2009) 17-27.

[50] J. Zurdo, J.I. Guijarro, C.M. Dobson, Preparation and characterization of purified amyloid fibrils, J Am Chem Soc, 123 (2001) 8141-8142.

Figure legends

Figure 1. Ovalbumin purification (Mw - molecular weight markers; OG - ovoglobulins' ammonium-sulphate precipitate and OA - purified ovalbumin); a) SDS PAGE following the purification process; b) RP-HPLC chromatogram of purified ovalbumin.

Figure 2. a) ThT fluorescence of ovalbumin samples incubated at low pH and high temperature in 24-hour interval; b) ANS fluorescence of ovalbumin incubated in the same conditions. Each value is the average of the results of three experiments, and the error bars show the standard deviations; c) AFM microscopy of ovalbumin sample incubated 24 hours in low-pH, high-temperature conditions.

Colour should be used for this figure in print

Figure 3. a) SDS PAGE of ovalbumin samples incubated at low pH and elevated temperatures for 0, 2, 4, and 24 hours; b) densitometry analysis of monomeric ovalbumin band (45 kDa). Each value is the average of the results of triplicates, and the error bars show the standard deviations

Figure 4. Amide I region of ovalbumin samples incubated at pH 2, 90°C for 0-24 hours.

Colour should be used for this figure in print

Figure 5. Second derivatives of IR spectra in Amide I region of ovalbumin samples incubated at pH 2, 90°C for 0-24 h.

Figure 6. Amide II region of native ovalbumin (pH 7, 0h), and samples incubated at pH 2, 90°C for 0-24 hours.

Colour should be used for this figure in print

Figure 7. Amide III region of native ovalbumin (pH 7, 0h), and samples incubated at pH 2, 90°C for 0-24 hours.

Colour should be used for this figure in print

Figure 8. Changes in aggregation specific β-sheet content during incubation of ovalbumin at low pH and elevated temperature, a) low (1625 cm^{-1}) and b) high (1695 cm^{-1}) frequency. Correlation between ThT fluorescence intensities and aggregation specific β-sheet content, c) low (1625 cm^{-1}) and d) high (1695 cm^{-1}) frequency.

Figure 9. Changes in normalized intensities of aggregation specific β-sheet bands based on the Amide I/Amide II ratio during incubation of ovalbumin at low pH and elevated temperature, a) low (1625 cm^{-1}) and b) high (1695 cm^{-1}) frequency. Correlation between ThT fluorescence intensities and Amide I/Amide II ratio, c) low (1625 cm^{-1}) and d) high (1695 cm^{-1}) frequency.

Author contributions:
J.M., and J.P. conceived and conducted the experiments, J.M., B.J., B.J. and N.P. analyzed the results, and revised the manuscript. All authors reviewed and approved the manuscript

Declaration of interests

☒ The authors declare that they have no known competing financial interests or personal relationships that could have appeared to influence the work reported in this paper.

☐The authors declare the following financial interests/personal relationships which may be considered as potential competing interests:

None.

Highlights

- Mature ovalbumin amyloid fibrils are obtained after only 24-hour at pH 2, 90°C
- In addition to Amide I, Amide III region offers qualitative fibrillation evidence.
- Second derivative spectrum is more sensitive in detecting structural transitions.
- Amide I/Amide II ratio is a facile method for quantitative fibrillation monitoring.

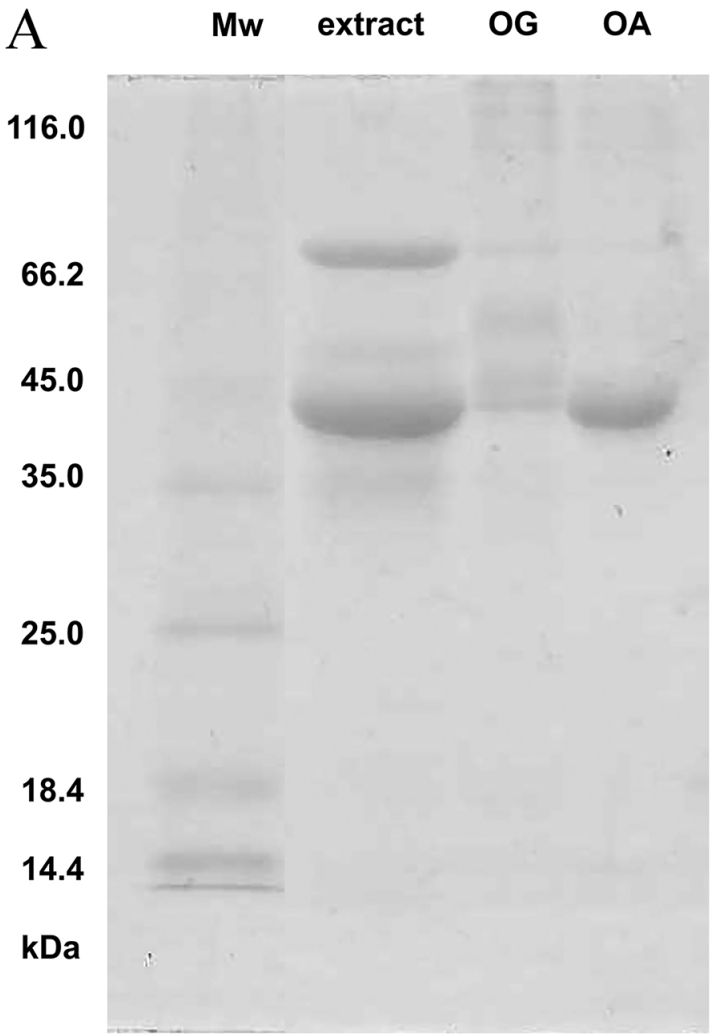
A
Mw
extract
OG
OA
116.0
66.2
45.0
35.0
25.0
18.4
14.4
kDa

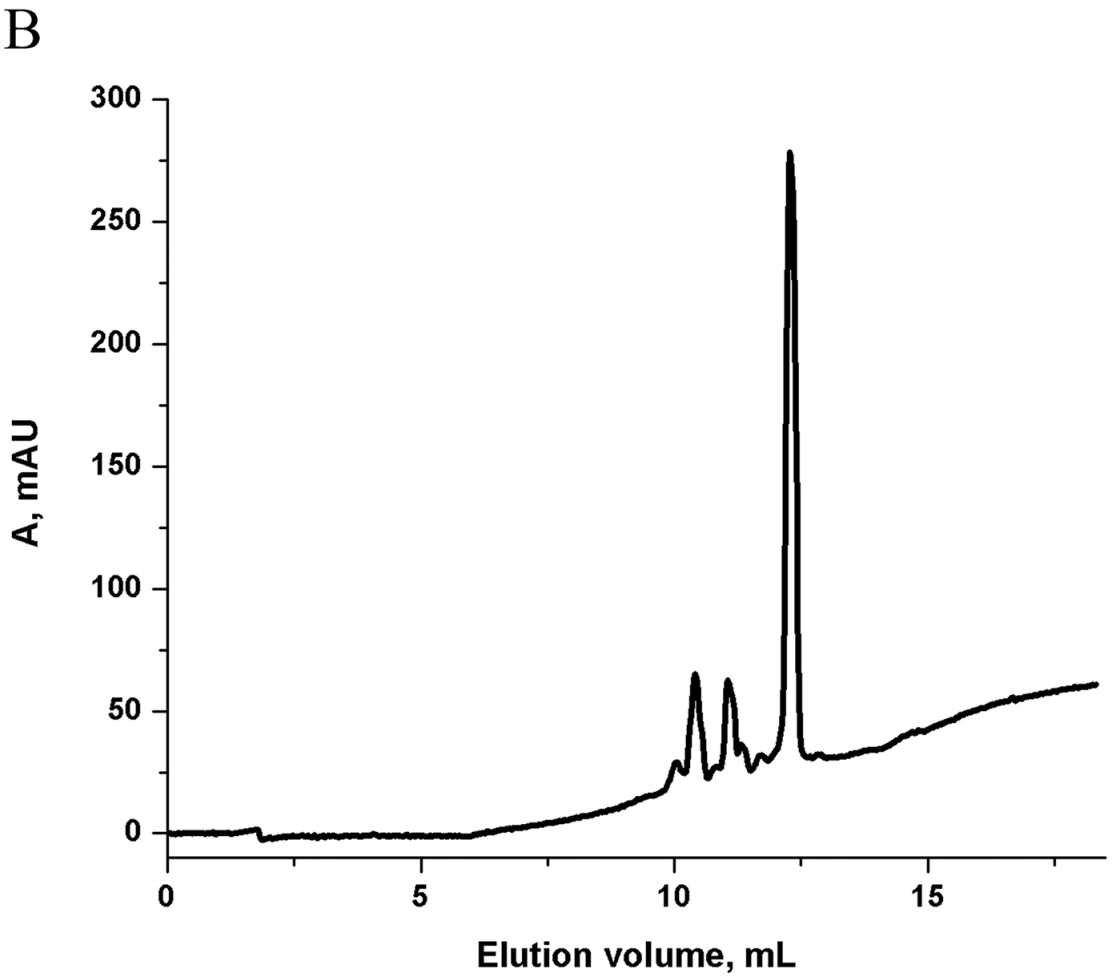
B
300
250
200
150
100
50
0
A, mAU
0
5
10
15
Elution volume, mL

Figure 1

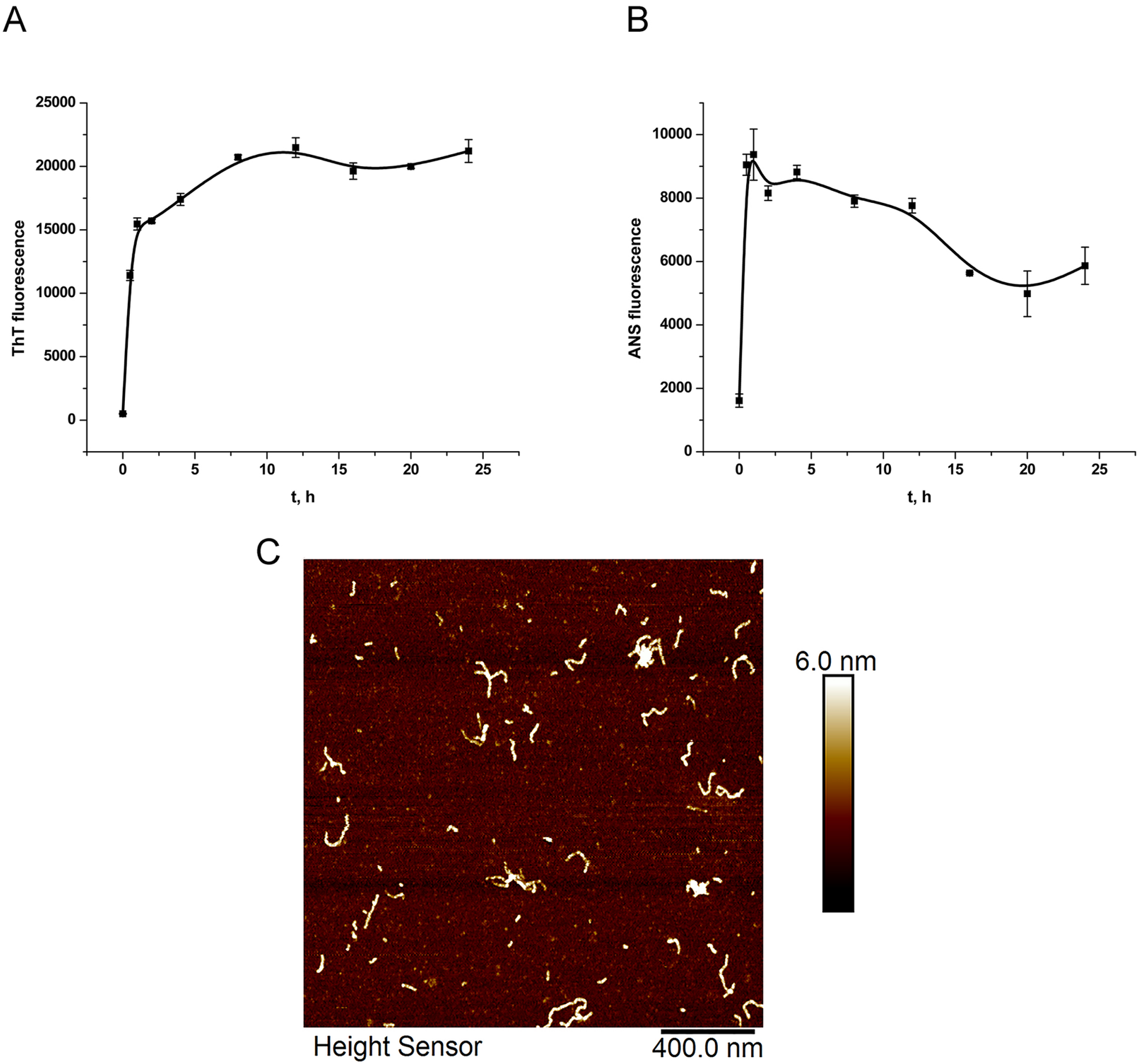
A
ThT fluorescence
t, h
B
ANS fluorescence
t, h
C
6.0 nm
Height Sensor
400.0 nm

Figure 2

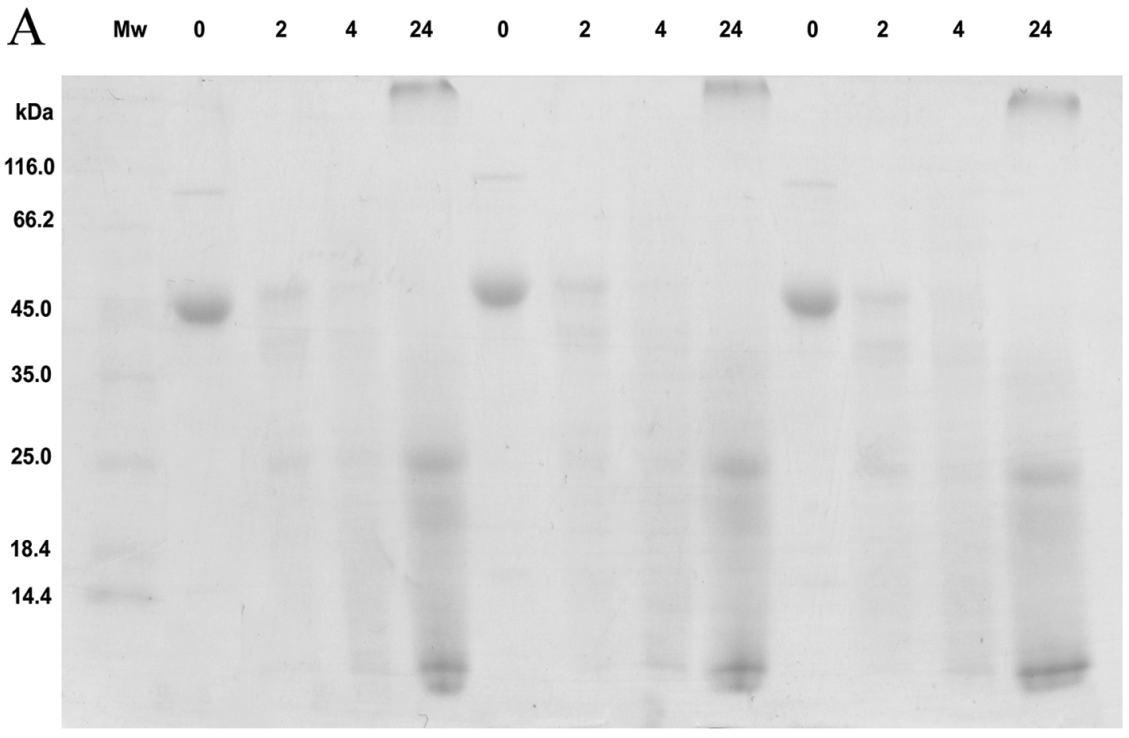
A
Mw
0
2
4
24
0
2
4
24
0
2
4
24
kDa
116.0
66.2
45.0
35.0
25.0
18.4
14.4

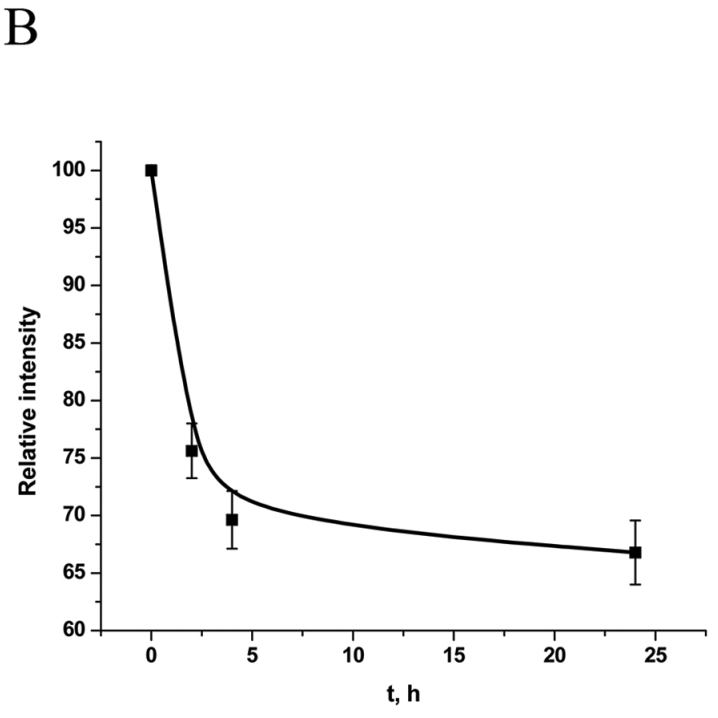
B
Relative intensity
100
95
90
85
80
75
70
65
60
0
5
10
15
20
25
t, h

Figure 3

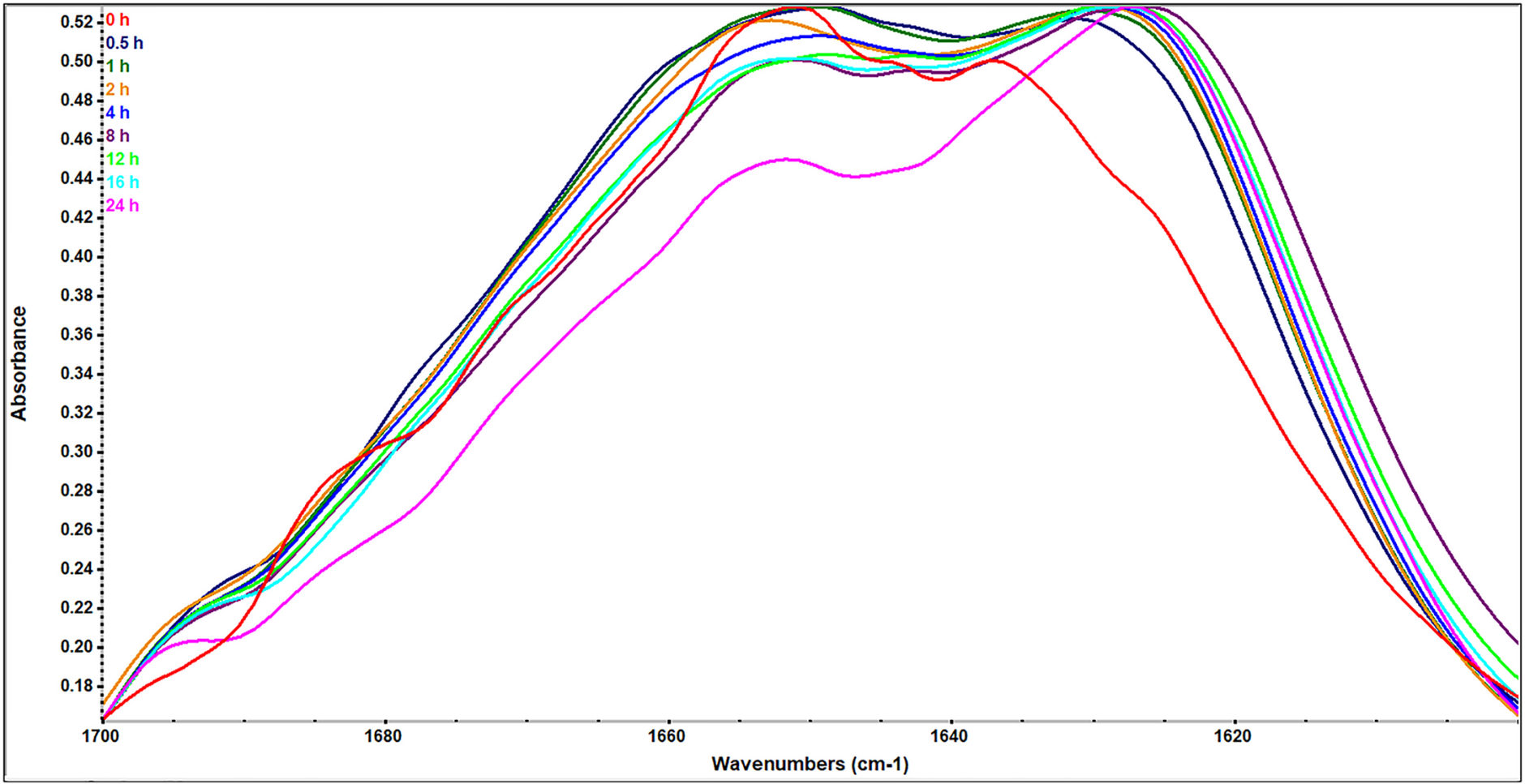
0 h
0.5 h
1 h
2 h
4 h
8 h
12 h
16 h
24 h
Absorbance
0.52
0.50
0.48
0.46
0.44
0.42
0.40
0.38
0.36
0.34
0.32
0.30
0.28
0.26
0.24
0.22
0.20
0.18
1700
1680
1660
1640
1620
Wavenumbers (cm-1)

Figure 4

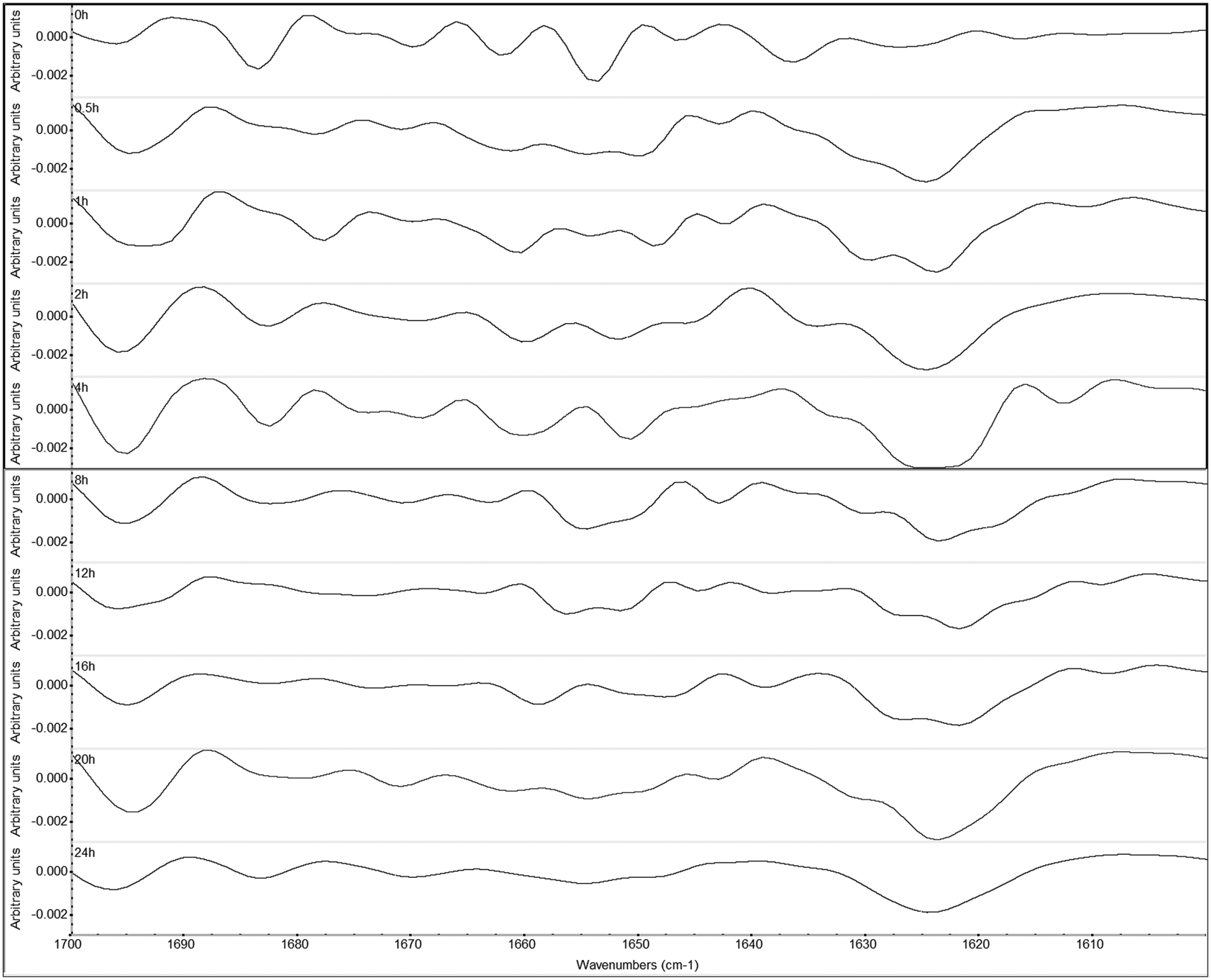
0h
0.5h
1h
2h
4h
8h
12h
16h
20h
24h
Arbitrary units
0.000
-0.002
1700
1690
1680
1670
1660
1650
1640
1630
1620
1610
Wavenumbers (cm-1)

Figure 5

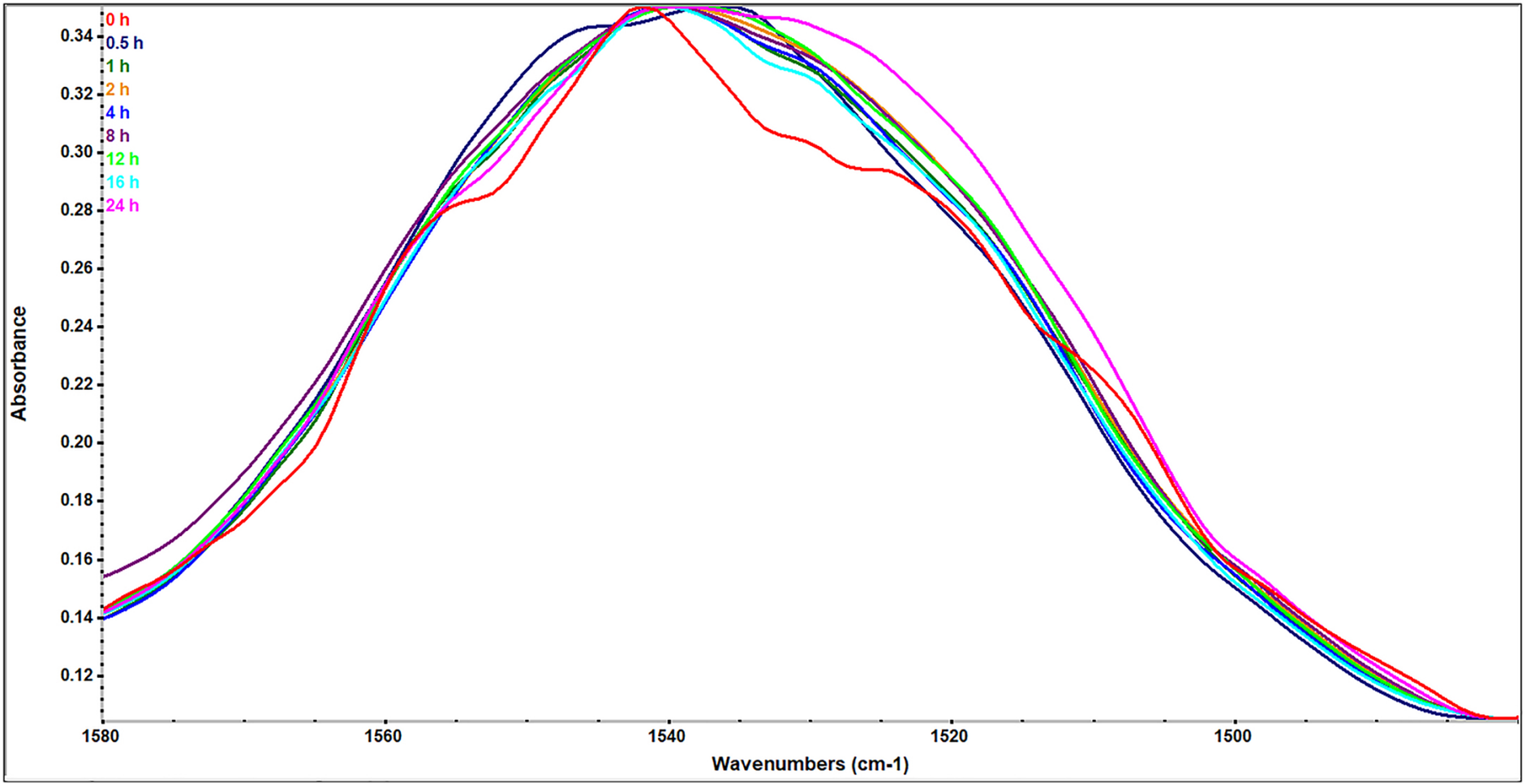
0 h
0.5 h
1 h
2 h
4 h
8 h
12 h
16 h
24 h
Absorbance
0.34
0.32
0.30
0.28
0.26
0.24
0.22
0.20
0.18
0.16
0.14
0.12
1580
1560
1540
1520
1500
Wavenumbers (cm-1)

Figure 6

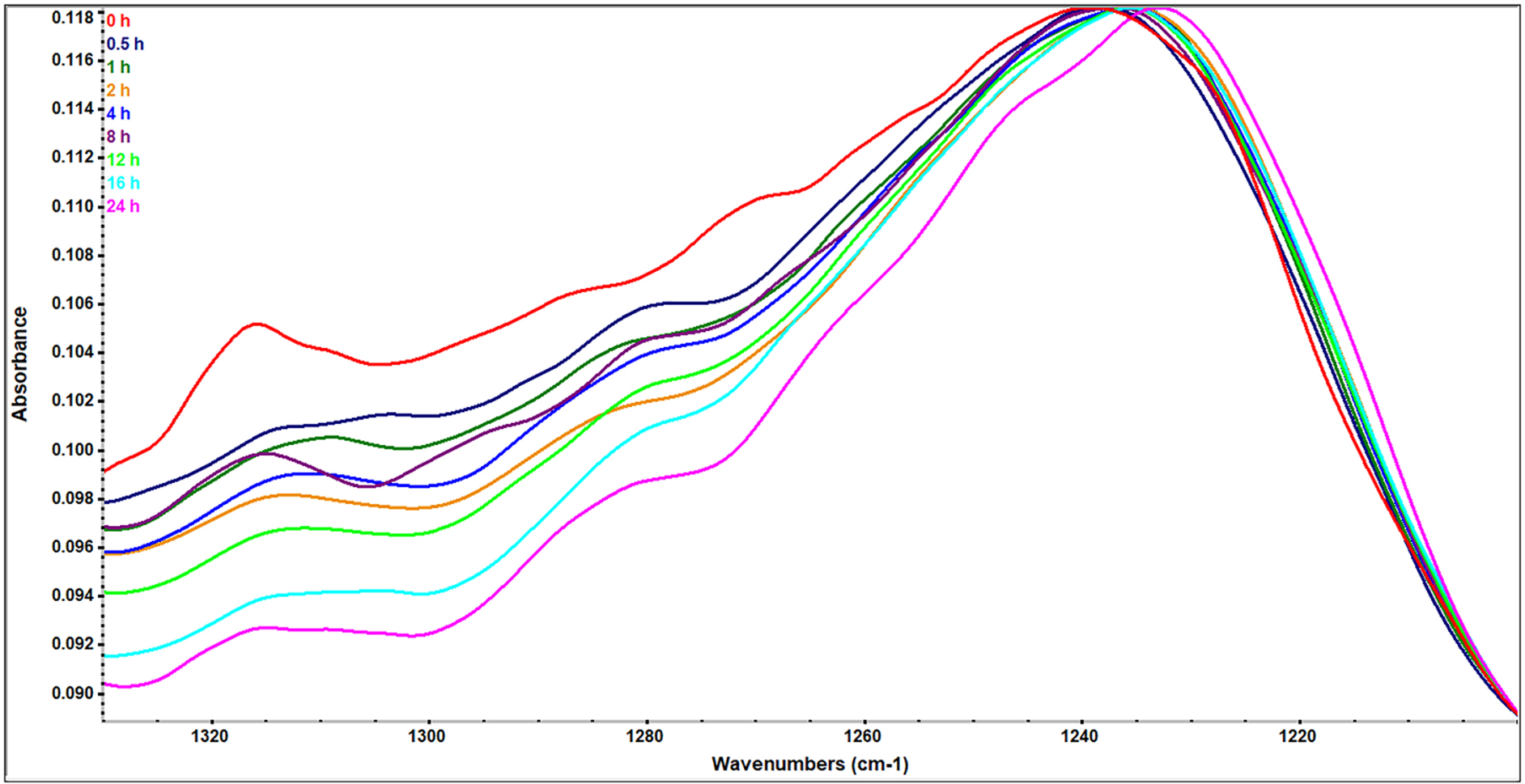
0 h
0.5 h
1 h
2 h
4 h
8 h
12 h
16 h
24 h
Absorbance
0.118
0.116
0.114
0.112
0.110
0.108
0.106
0.104
0.102
0.100
0.098
0.096
0.094
0.092
0.090
1320
1300
1280
1260
1240
1220
Wavenumbers (cm-1)

Figure 7

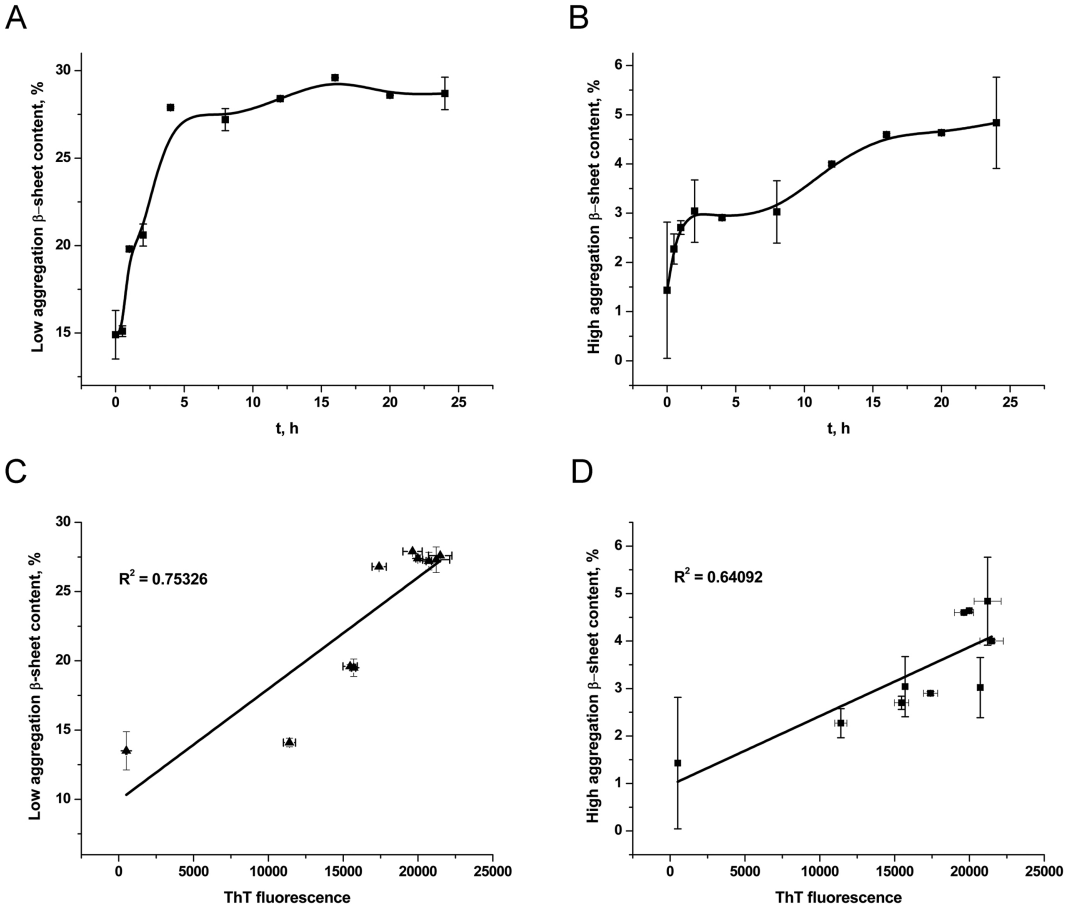
A
Low aggregation β-sheet content, %
t, h
B
High aggregation β-sheet content, %
t, h
C
Low aggregation β-sheet content, %
R² = 0.75326
ThT fluorescence
D
High aggregation β-sheet content, %
R² = 0.64092
ThT fluorescence

Figure 8

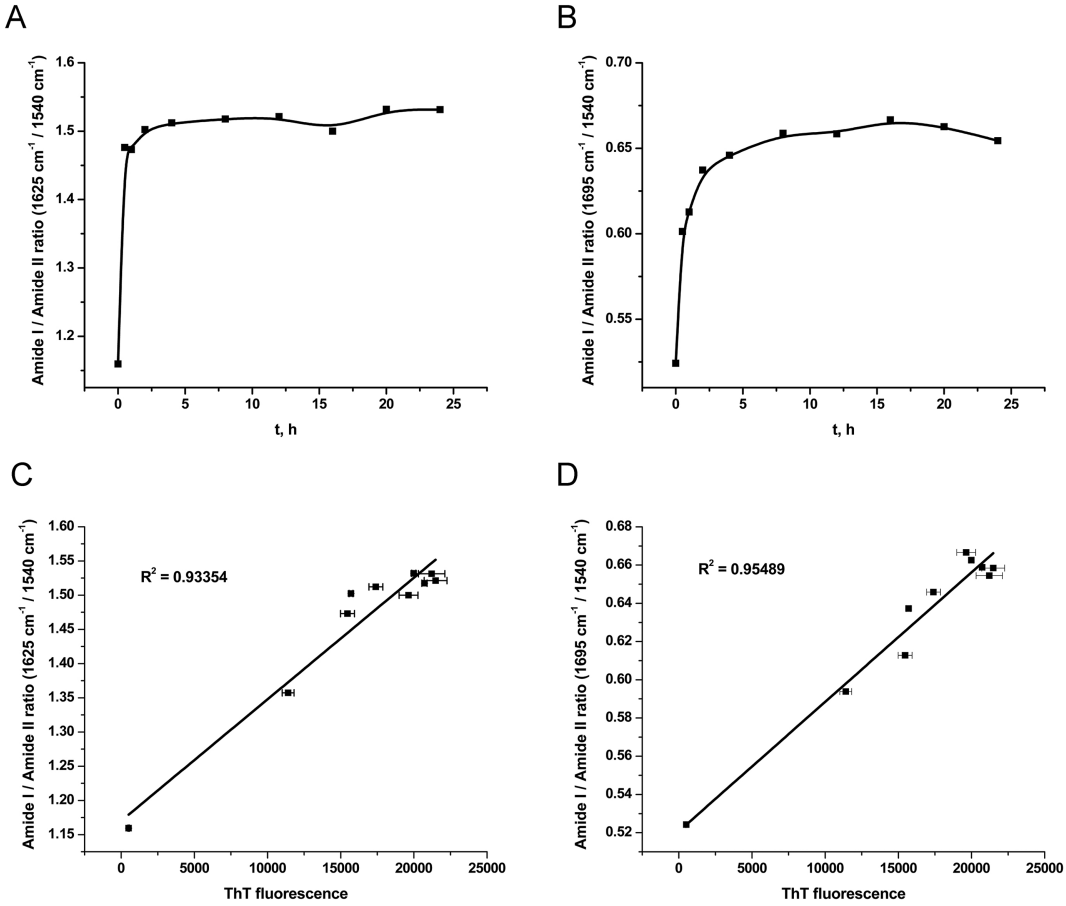
A
Amide I / Amide II ratio (1625 cm-1 / 1540 cm-1)
t, h
B
Amide I / Amide II ratio (1695 cm-1 / 1540 cm-1)
t, h
C
R2 = 0.93354
Amide I / Amide II ratio (1625 cm-1 / 1540 cm-1)
ThT fluorescence
D
R2 = 0.95489
Amide I / Amide II ratio (1695 cm-1 / 1540 cm-1)
ThT fluorescence

Figure 9